Mesoscopic superconductors in the London limit: Equilibrium properties and metastability

E. Akkermans,[1] D. M. Gangardt,[1] and K. Mallick[2]
[1]*Department of Physics, Technion, 32000 Haifa, Israel*
[2]*Service de Physique Théorique, CEA Saclay, 91191 Gif-Sur-Yvette, France*
(Received 19 August 2000; published 24 January 2001)

We present a study of the behavior of metastable vortex states in mesoscopic superconductors. Our analysis relies on the London limit within which it is possible to derive closed analytical expressions for the magnetic field and the Gibbs free energy. We consider in particular the situation where the vortices are symmetrically distributed along a closed ring. There, we obtain expressions for the confining Bean-Livingston barrier and for the magnetization which turns out to be paramagnetic away from thermodynamic equilibrium. At low temperature, the barrier is high enough for this regime to be observable. We propose also a local description of both thermodynamic and metastable states based on elementary topological considerations; we find structural phase transitions of vortex patterns between these metastable states and we calculate the corresponding critical fields.

DOI: 10.1103/PhysRevB.63.064523 PACS number(s): 74.25.Ha, 74.60.Ec, 74.80.−g

I. INTRODUCTION

A significant amount of work has been recently devoted to the study of aluminum superconducting disks in a mesoscopic regime, in which the size of the sample is comparable with both the coherence length ξ and the London penetration depth λ. In a first set of experiments[1] the magnetization of such systems was measured at thermodynamic equilibrium. Beyond the Meissner state, a series of discontinuous jumps appear when the applied magnetic field is increased. This behavior corresponds to the entrance of individual quantized vortices in the sample. A quantitative understanding of the phenomena involved can be achieved through a numerical study of the Ginzburg-Landau equations.[2–5] Analytical progress can be made if one considers special limits of these equations (such as the linear limit,[6] the London regime,[7,8] or the Bogomol'nyi dual point[9,10]). In later experiments,[11] it was noticed that when sweeping down the applied field the sample exhibits a paramagnetic Meissner effect, i.e., it has a paramagnetic magnetization. Such a behavior previously found in high-T_c superconductors[12] had been interpreted as a special feature of these materials. However, its occurrence in aluminum disks calls for a less specific explanation which results from the role played by metastable states at temperatures well below the critical temperature.[13]

This work is devoted to the study of metastable states in a mesoscopic superconductor. We shall investigate vortex patterns in a thin cylinder placed in a magnetic field parallel to its axis. Our analysis will be carried on in the London regime, i.e., in the limit $\kappa \gg 1$, where κ is the Ginzburg-Landau parameter. Using known results[14] for the magnetization of an infinite cylinder with a circular cross section of radius R, we derive, in the mesoscopic regime (i.e., when the London length is much larger than R), closed expressions for the magnetic field and the free energy that are suitable for analytical calculations. They allow us to obtain the Bean-Livingston barrier and to calculate the series of matching fields (critical fields corresponding to the entrance of the Nth vortex). The paramagnetic Meissner state can then be explained using a simple scenario for the hysteretic behavior of the magnetization, involving the appearance and the disappearance of the surface barrier.

Once the existence of metastable states is established, a criterion to classify them is required. The number of vortices is a simple topological number but it is not precise enough to distinguish between all different types of states. Projection methods into eigenstates of the linearized theory produce a set of integers that were proposed as classifying numbers to characterize a given metastable vortex state[5] and that would generalize quantum numbers to a nonlinear theory. However, these numbers are nongeneric and it is not obvious to relate them to the geometric features of a given pattern. A more geometrical path will be followed here to present a topological description of vortex patterns. Our study is based on an analogy between a configuration of vortices and a dynamical system, obtained by interpreting the superconducting current as the local (phase-space) velocity of a particle. The Hamiltonian of the associated dynamical system turns out to be the magnetic field. We shall show that a configuration of vortices can be characterized by the critical points of the magnetic field (or equivalently the points where the current vanishes). The number of critical points of a given type (maxima, minima, saddle points) will provide a natural set of topological invariant integers associated with a configuration. This geometrical analysis reveals the existence of structural transitions between states with the *same* number of vortices: indeed, the number and the nature of the critical points can vary abruptly when the applied field exceeds some specific values, inducing topological phase transitions.[15] For a simple polygonal configuration of vortices, we calculate the corresponding transition fields. These topological changes are in fact best visualized using a ''dual'' description of a system of vortices, closely related to the paramagnetic Meissner effect: there exists a special closed curve Γ, first introduced in Ref. 10, which is everywhere orthogonal to the current lines and which passes through the critical points of the system. Therefore any structural change affecting the critical points, will manifest itself in a topological change of the shape of Γ. This curve thus provides an efficient and elegant tool to characterize vortex patterns and to understand qualitatively the

topological transitions between different configurations.

The plan of this article goes as follows. In Sec. II, we recall how the London free energy can be obtained as a limit of the Ginzburg-Landau theory. In Sec. III, we present the solution of London equation in the case of an infinite circular cylinder (details of the calculations are given in Appendixes A and B). Section IV is devoted to the mesoscopic limit: we calculate the magnetic field and the free energy, study the Bean-Livingston barrier, and obtain the matching fields. The paramagnetic Meissner state is obtained in Sec. V. Section VI is devoted to the topological investigation of vortex patterns: we show that the critical points characterize a configuration and we demonstrate the existence of topological phase transitions. In the second part of Sec. VI, the dual description of a configuration of vortices, via the curve Γ, is introduced to provide a better understanding of the transitions between patterns. Section VII contains some concluding remarks and discussions.

II. LONDON LIMIT OF THE GINZBURG-LANDAU EQUATIONS

Consider an infinite superconducting cylinder with a cross section of area Ω in the constant magnetic field $h_e\hat{z}$ along the axis of the cylinder. In the presence of a magnetic field the Ginzburg-Landau free energy density per unit length of the cylinder, defined as difference of free energies with and without magnetic field $\mathcal{F}=F_S(h)-F_S(0)$, reads

$$\mathcal{F}=\int\left(\frac{\vec{h}^2}{2}+\kappa^2(1-|\psi|^2)^2+|(\vec{\nabla}-i\vec{A})\psi|^2\right)d^2r, \quad (1)$$

where $\psi=|\psi|e^{i\chi}$ is the order parameter and $\vec{h}=\vec{\nabla}\times\vec{A}$ is the local magnetic induction. The integration is performed over the cross section of the cylinder. A superconductor is characterized by two length scales: the London penetration depth λ and the coherence length ξ. The Ginzburg-Landau parameter is defined as their ratio $\kappa=\lambda/\xi$. In this work lengths are measured in units of $\lambda\sqrt{2}$ and the magnetic induction in units of the thermodynamic critical field $H_c=\phi_0/2\sqrt{2}\pi\lambda\xi$, where $\phi_0=hc/2e$ is the magnetic flux quantum. The free energy (1) is given in units of $\xi^2H_c^2/4\pi$.

The Ginzburg-Landau equations for ψ and $\vec{h}$ are obtained from a variation of $\mathcal{F}$. They are given by

$$-(\vec{\nabla}-i\vec{A})^2\psi=2\kappa^2\psi(1-|\psi|^2), \quad (2)$$

$$\vec{\nabla}\times\vec{h}=2|\psi|^2(\vec{\nabla}\chi-\vec{A}). \quad (3)$$

Equation (3) is the Maxwell-Ampère equation which could be written as well using the current density $\vec{J}=\mathrm{Im}(\psi^*\vec{\nabla}\psi)-|\psi|^2\vec{A}$. Outside the superconducting sample, $\psi=0$. The boundary condition suitable for a superconductor/insulator interface is[16]

$$(\vec{\nabla}-i\vec{A})\psi|_{\hat{n}}=0; \quad (4)$$

here $\hat{n}$ is the unit vector normal at each point to the surface of the superconductor.

We study a superconductor in an applied external field h_e; the relevant thermodynamic potential is the Gibbs free energy G obtained from F via a Legendre transformation

$$G=F-\Omega h_eB, \quad (5)$$

where the total (dimensionless) magnetic induction (in the $\hat{z}$; direction) B is given by the averaging the magnetic induction over the cross section

$$B=\frac{1}{\Omega}\int h(\vec{r})d^2r, \quad (6)$$

where the magnetic induction is always in $\hat{z}$ direction: $\vec{h}=h\hat{z}$.

In the normal phase, we have $\psi=0$, $B=h_e$, and $F_S(h)=F_N(h)=\Omega h^2/2$. Therefore the corresponding Gibbs free energy G_N is given by

$$G_N=F_N(h)-\Omega h_eB=F_N(0)-\frac{\Omega h_e^2}{2}. \quad (7)$$

At thermodynamic equilibrium, the superconductor selects the state of minimal Gibbs free energy. The quantity which is measured in experiments is the magnetization M of the superconductor due to the applied field given by $4\pi M=B-h_e$. It is obtained at thermodynamic equilibrium using the thermodynamic relation[16]

$$-M=\frac{1}{2\pi}\frac{\partial\mathcal{G}}{\partial h_e}, \quad (8)$$

where the difference of the (dimensionless) Gibbs energies $\mathcal{G}=G_S-G_N$ up to a constant equal to the superconducting condensation energy, is given by

$$\mathcal{G}=\mathcal{F}-\Omega h_eB+\Omega h_e^2/2. \quad (9)$$

The dimensionless ratio $\kappa=\lambda/\xi$ is the only free parameter to describe the superconducting state. It determines, in the limit of an infinite system, whether the sample is a type-I or type-II superconductor.[16] For $\kappa\geqslant 1/\sqrt{2}$, i.e., for type-II superconductors, it is energetically favorable for the system in a large enough magnetic field to sustain normal regions in the bulk which appear as vortices. We shall now study the system of vortices in an extreme type-II superconductor, i.e., in the London limit $\kappa\gg 1$.

In this limit, the amplitude of the order parameter $|\psi|$ does not vary and can be taken equal to one except at the position of the vortices where $|\psi|$ vanishes. The Ginzburg-Landau free energy reduces to

$$\mathcal{F}=\int\left[\frac{h^2}{2}+|(\vec{\nabla}-i\vec{A})\psi|^2\right]d^2r. \quad (10)$$

Using Eq. (3) and $|\psi|^2=1$ almost everywhere (except at the position of the vortices), we can write

$$|(\vec{\nabla}-i\vec{A})\psi|^2=(\vec{\nabla}\times\vec{h})^2 \quad (11)$$

so that the free energy is given by the expression

$$\mathcal{F}=\frac{1}{2}\int\left[h^2+\frac{1}{2}(\vec{\nabla}\times\vec{h})^2\right]d^2r \tag{12}$$

which in our units is independent of κ. To obtain the equation for h, we notice that the phase χ of the order parameter is nonsingular except near a vortex (say at $r=0$) where it has the property that

$$\oint\vec{\nabla}\chi\cdot\vec{dl}=2\pi \tag{13}$$

on any closed contour encircling the singularity at point $r=0$. Using Stokes theorem,

$$\oint\vec{\nabla}\chi\cdot\vec{dl}=\int\int d\vec{S}\cdot\vec{\nabla}\times\vec{\nabla}\chi=2\pi, \tag{14}$$

we deduce that the $\hat{z}$ component of $\vec{\nabla}\times\vec{\nabla}\chi$ equals $2\pi\delta(\vec{r})$. The equation for h is then obtained by taking the curl of Eq. (3) and using that $|\psi|^2=1$ almost everywhere:

$$\nabla^2h-2h=-4\pi\delta(\vec{r}). \tag{15}$$

This equation can be generalized to the case of N vortices placed at points $\vec{r}_k$

$$\nabla^2h-2h=-4\pi\sum_{k=1}^{N}\delta(\vec{r}-\vec{r}_k). \tag{16}$$

In the next section we shall present the solution of this equation in the particular case of a cylinder with circular cross section.

III. SOLUTION FOR *N* VORTICES IN A CIRCULAR CYLINDER

From now on we shall study a circular cylinder of radius R. The magnetic induction and Gibbs energy of a system of N vortices in this geometry has been studied in Ref. 14. The detailed derivation of the results is presented in Appendix A. The solution $h(r,\theta)$ of Eq. (16) satisfying the boundary condition $h(R,\theta)=h_e$ can be written as a sum of three terms:

$$h(r,\theta)=h_M(r)+h_V(r,\theta)+h_{\overline{V}}(r,\theta). \tag{17}$$

The first term

$$h_M(r)=h_eI_0(\sqrt{2}r)/I_0(\sqrt{2}R), \tag{18}$$

where $I_0(x)$ is the modified Bessel function of first kind, describes the Meissner effect in the absence of vortices. The second term is the magnetic induction of N vortices placed at points $\vec{r}_k=(r_k,\theta_k)$ for $k=1,\ldots,N$ and it is given by

$$h_V(r,\theta)=2\sum_{k=1}^{N}K_0(\sqrt{2}|\vec{r}-\vec{r}_k|). \tag{19}$$

The third term, written with help of the modified Bessel function of first and second kind $I_n(x),K_n(x)$ as

$$h_{\overline{V}}(r,\theta)=-2\sum_{n=-\infty}^{+\infty}K_n(\sqrt{2}R)\frac{I_n(\sqrt{2}r)}{I_n(\sqrt{2}R)}\times\sum_{k=1}^{N}I_n(\sqrt{2}r_k)\cos n(\theta-\theta_k), \tag{20}$$

ensures the boundary condition $h(R,\theta)=h_e$. We are interested in polygonal rings of vortices. For this particular configuration $r_k=d,\theta_k=2\pi k/N$ and the expression for $h_{\overline{V}}(r,\theta)$ can be simplified,

$$h_{\overline{V}}(r,\theta)=-2N\sum_{n=-\infty}^{+\infty}K_n(\sqrt{2}R)\times\frac{I_n(\sqrt{2}r)I_n(\sqrt{2}d)}{I_n(\sqrt{2}R)}\cos Nn\theta. \tag{21}$$

The corresponding Gibbs energy has also been obtained in Ref. 14 The expression of the dimensionless Gibbs energy is given by

$$\mathcal{G}=\mathcal{F}-h_e\int h(\vec{r})d^2r+\pi R^2h_e^2/2. \tag{22}$$

The field h_V diverges at the positions of the vortices and the corresponding part of the free energy must be regularized. The singular contribution coincides with one calculated by Abrikosov[17] for the case of infinite system and is given by

$$\mathcal{F}_\infty=N\mathcal{E}+2\pi\sum_{j\neq k}K_0(\sqrt{2}|\vec{r}_j-\vec{r}_k|), \tag{23}$$

where $\mathcal{E}=2\pi(\ln\kappa+0.081)$ is the one-vortex energy.

The regular part of the Gibbs energy is calculated in Appendix B. Using the expressions (18), (19), and (20) for the magnetic field, one obtains

$$\mathcal{G}_N-\mathcal{G}_0=N\mathcal{E}+2\pi\sum_{j\neq k}K_0(\sqrt{2}|\vec{r}_j-\vec{r}_k|)-2\pi h_e\times\sum_{k=1}^{N}\left(1-\frac{I_0(\sqrt{2}r_k)}{I_0(\sqrt{2}R)}\right)-2\pi\sum_{n=-\infty}^{+\infty}\sum_{i,j=1}^{N}\frac{K_n(\sqrt{2}R)I_n(\sqrt{2}r_i)I_n(\sqrt{2}r_j)}{I_n(\sqrt{2}R)}\times\cos n(\theta_i-\theta_j), \tag{24}$$

where $\mathcal{G}_0=\pi Rh_e^2[R/2-(\sqrt{2}/2)I_1(\sqrt{2}R)/I_0(\sqrt{2}R)]$ is the Gibbs energy in the absence of vortices, i.e., in the Meissner state. For the particular case of vortices distributed on a regular polygon of radius d, the previous expression (24) simplifies and becomes

$$\frac{\mathcal{G}_N-\mathcal{G}_0}{N}=\mathcal{E}+2\pi\sum_{l=1}^{N-1}K_0\left(\left|2\sqrt{2}d\sin\frac{l\pi}{N}\right|\right)-2\pi h_e\left(1-\frac{I_0(\sqrt{2}d)}{I_0(\sqrt{2}R)}\right)-2\pi N\sum_{n=-\infty}^{+\infty}\frac{K_{Nn}(\sqrt{2}R)I_{Nn}(\sqrt{2}d)^2}{I_{Nn}(\sqrt{2}R)}. \quad (25)$$

Similar expressions have been already obtained previously in Refs. 14 and 8 and we shall now discuss them in the limit of a small radius R in order to use the particularly elegant structure of the corresponding solutions to derive analytical expressions for the magnetic field and the energy.

IV. CASE OF A MESOSCOPIC CYLINDER

We shall now consider the limiting case where $R\ll\lambda$ for which the corresponding Gibbs free energy was obtained in Ref. 7. In this limit the previous expressions greatly simplify. Since all the distances are given in units of $\lambda\sqrt{2}$, we can expand the expression for the magnetic induction using the expansion of the Bessel functions for small argument, so that

$$h(z,\bar{z})-h_e=\phi_e(|z|^2-1)+2\sum_{i=1}^{N}\ln\left|\frac{1-\bar{z}_i z}{z-z_i}\right|, \quad (26)$$

where $\phi_e=h_eR^2/2$ is the flux of the external field through the system and we use the complex notations

$$z=\left(\frac{r}{R}\right)e^{i\theta}\quad\text{and}\quad z_k=\left(\frac{r_k}{R}\right)e^{i\theta_k} \quad (27)$$

together with complex conjugate $\bar{z}$ and $\bar{z}_k$. This expression for the magnetic induction is solution of the modified London equation

$$\frac{\partial^2}{\partial z\partial\bar{z}}h(z,\bar{z})-h_e=-\pi\sum_{i=1}^{N}\delta(z-z_i)\delta(\bar{z}-\bar{z}_i) \quad (28)$$

which can be obtained from Eq. (16) for small variation of the field on the scale of R.

In the particular case, we shall consider from now on, of vortices distributed along a regular polygon of radius d, we have $r_k=d$ and for the N vortices sitting on a shell, the angle θ_k of the kth vortex is $\theta_k=2\pi k/N$. Then, defining the real quantity $x=d/R\leqslant 1$, the relation (26) becomes

$$h_N(z,\bar{z})-h_e=\phi_e(|z|^2-1)+2\ln\left|\frac{1-x^Nz^N}{x^N-z^N}\right|, \quad (29)$$

whereas the Gibbs energy (25) becomes

$$\frac{\mathcal{G}_N-\mathcal{G}_0}{N}=\mathcal{E}'-2\pi\phi_e(1-x^2)+2\pi\ln(1-x^{2N})-2\pi(N-1)\ln x-2\pi\ln N, \quad (30)$$

where $\mathcal{G}_0=\pi\phi_e^2/2$ and $\mathcal{E}'\simeq 2\pi\ln(R/\xi)$.

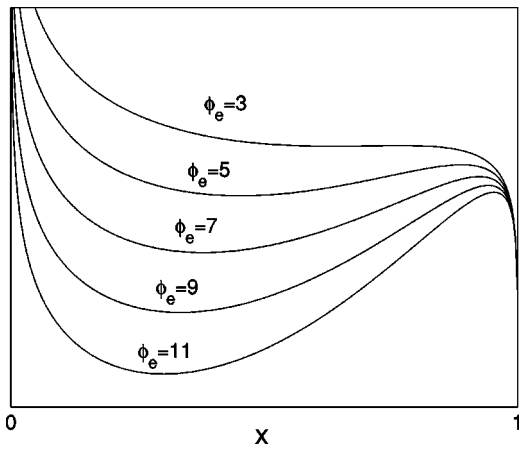

FIG. 1. Behavior of the Gibbs energy as a function of the position x of the $N=3$ vortex shell. The maximum which exists for high enough applied field corresponds to the unstable equilibrium point for the vortex configuration and gives the height of the Bean-Livingston barrier.

The relation between the radius x of the polygonal configuration and the external flux ϕ_e is obtained by minimizing $\mathcal{G}_N(x,h_e)$ with respect to x at fixed ϕ_e, namely

$$\phi_e=\frac{N-1}{2x^2}+\frac{Nx^{2N-2}}{1-x^{2N}}. \quad (31)$$

A. The Bean-Livingston barrier

The relation (31) has, as a function of the applied flux ϕ_e, either zero, one or two solutions. The latter case corresponds for the Gibbs energy (30) to the existence of a Bean-Livingston potential barrier[18,19] for which one solution is stable and gives the equilibrium position of the vortices while the second solution is unstable and gives the height of the potential barrier as shown in Fig. 1. It should be noticed that for more than one vortex ($N>1$), the energy $\mathcal{G}_N$ diverges logarithmically at the origin $x=0$ due to the repulsion between the vortices.

The potential barrier disappears for low enough applied flux below a characteristic value ϕ_{min} given by the minimum of the function $f_N(x)$ in the right-hand side (rhs) of Eq. (31) as represented in Fig. 2. Defining $y=x^2$, we have

$$f_N(y)=\frac{N-1}{2y}+\frac{Ny^{N-1}}{1-y^N}, \quad (32)$$

$$f_N'(y)=-\frac{N-1}{2y^2}+\frac{N(N-1)y^{N-2}}{1-y^N}+\frac{N^2y^{2N-2}}{(1-y^N)^2}. \quad (33)$$

For large values of N, we have $y_{min}^N\simeq 1/2N$ so that

$$\phi_{min}\simeq\frac{N-1}{2\sqrt[N]{2N}}\simeq\frac{N-1}{2}. \quad (34)$$

For $\phi_e<\phi_{min}$, there is no stable solution and then no equilibrium position for N vortices exists.

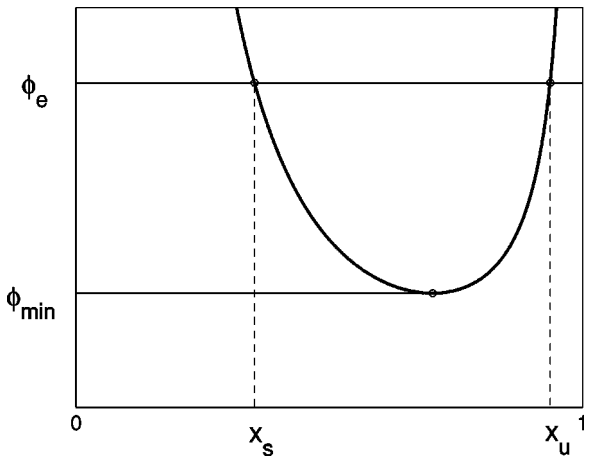

FIG. 2. Graphical solution of Eq. (31). The curve shows the behavior of $\phi_e(x)$. The two solutions x_s and x_u correspond respectively to the stable and unstable positions of the vortex shell for values of the magnetic field above ϕ_{min}.

B. Matching fields

By plugging the expression (31) into the expression (30), we obtain the behavior of the Gibbs energy for N vortices as a function of the applied flux ϕ_e. This expression is the counterpart, in the London limit, of the parabolae obtained at the Bogomoln'yi point[10] for $\kappa=1/\sqrt{2}$. For a given value ϕ_e of the applied field, the optimal number of vortices corresponds to the envelope of the set of curves $\mathcal{G}_N(\phi_e)$ as represented in Fig. 3. The matching values ϕ_N are the values taken by the flux of the external field at which $\mathcal{G}_{N-1}(\phi_N)=\mathcal{G}_N(\phi_N)$. They correspond to the transition between configurations with $N-1$ and N vortices, respectively.

Using the relation (30), it is straightforward to obtain the field at which the first vortex penetrates the system; it is given by $\phi_1=\mathcal{E}'/2\pi=\ln(R/\xi)$. This field is larger than the field at which the Bean-Livingston potential barrier disappears. For larger values of N, in the limit $\phi_e \gg \phi_{min}$, we approximate the relation (31) by $\phi_e=(N-1)/2x^2$ so that

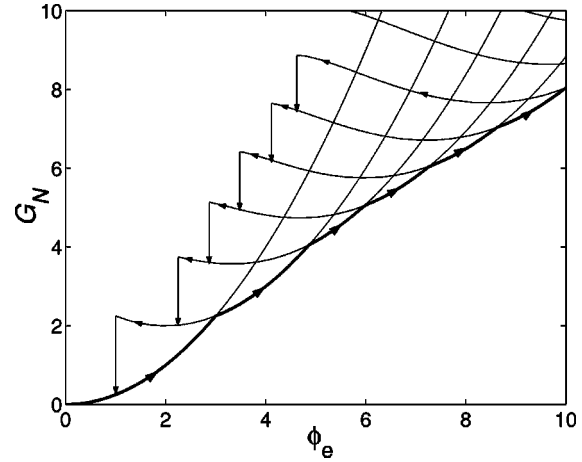

FIG. 3. Dependence of the Gibbs energy as a function of the applied flux ϕ_e. The equilibrium behavior of the system is described by the envelope of the curves for $\mathcal{G}_N(h_e)$. Arrows show the direction in which the magnetic flux is varied.

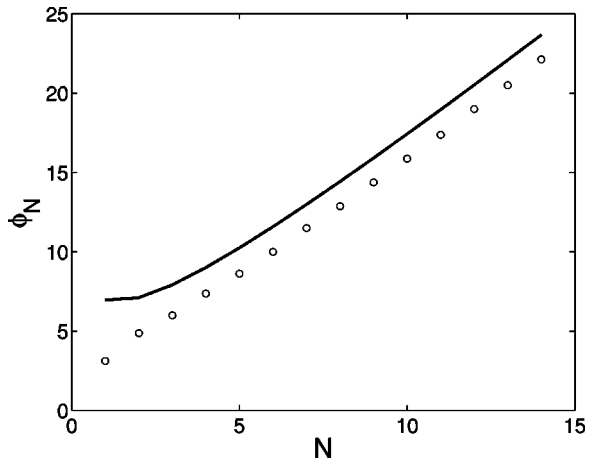

FIG. 4. Comparison between the relation (39) for the matching fields ϕ_N (solid line) and the numerical results (circles) for $\phi_1=\ln(R/\xi)=3$.

$$\frac{\mathcal{G}_N-\mathcal{G}_0}{2\pi}\approx N(\phi_1-\phi_e)+\frac{N(N-1)}{2}\left(1+\ln\frac{2\phi_e}{N-1}\right)-N\ln N. \tag{35}$$

Equating this to the similar expression for $\mathcal{G}_{N-1}(\phi_e)$ we obtain that the matching fields for $N\to\infty$ are given by solution of the following equation:

$$\phi_N=\phi_1+\frac{N-1}{2}\left(1+2\ln\frac{2\phi_N}{N}\right)-\ln N+1+\mathcal{O}(1/N). \tag{36}$$

We use the following ansatz $\phi_N=\frac{1}{2}(aN+b\ln N+c)$. Substituting it to Eq. (36) we obtain the coefficients

$$b=-\frac{2a}{a-2},\quad c=\frac{2a}{a-2}\left(1+\phi_1-\frac{a}{2}\right), \tag{37}$$

where the coefficient a satisfies the transcendental equation

$$a=1+2\ln a. \tag{38}$$

This equation has one obvious solution $a=1$ which is compatible with Eq. (36). However, from the exact numerical calculations of the matching fields using the relation (31) we infer that the second root $a\simeq 3.5129$ is realized in the solution for the matching fields. It leads to the formula

$$\phi_N=1.76N-2.32\ln N+2.32\phi_1-1.76+\mathcal{O}[(\ln N)^2/N]. \tag{39}$$

In Fig. 4 the values of the matching fields obtained from the computed free energy are compared with our prediction. The discrepancy is attributed to the slow convergence due to the term $\mathcal{O}[(\ln N)^2/N]$.

C. Magnetization and paramagnetic Meissner effect

A paramagnetic behavior for the total magnetization results from the existence of a high enough Bean-Livingston barrier and the long life-time of the corresponding metastable states. We propose the following scenario for the hys-

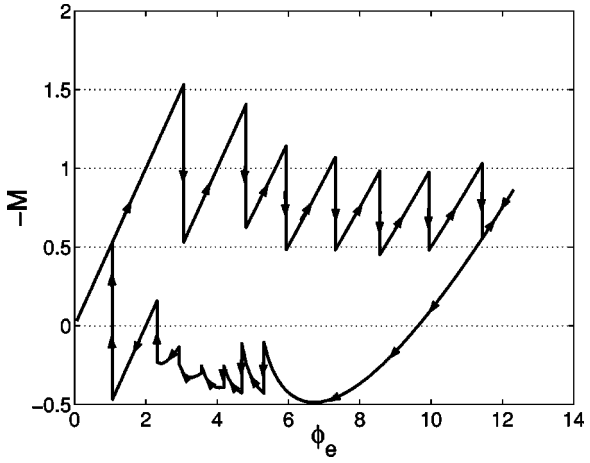

FIG. 5. Magnetization of the disk as a function of flux ϕ_e for $\phi_1=\ln(R/\xi)=3$. The hysteretic behavior is indicated by the arrows.

teretic behavior of the magnetization when the magnetic field is increased and then swept down.

If thermal equilibrium is maintained while increasing slowly the external flux ϕ_e, the results of the preceding section hold and the magnetization is given by the derivative of the envelope of the curves $\mathcal{G}_N(\phi_e)$ according to the thermodynamic relation (8). This behavior corresponds to the upper curve in Fig. 5.

When the applied field is decreased, the vortices that are already in the system are confined by the Bean-Livingston barrier and cannot escape the sample until the flux ϕ_e reaches a certain minimum value at which the barrier can be overcome, for instance, by the effect of thermal fluctuations. For the present discussion we use the ultimate criterion of zero barrier as a definition of the transition field.

From the discussion of Sec. IV A, we deduced that the potential barrier for N vortices disappears for a characteristic field given for large N by the relation (34), $\phi_{min}\sim(N-1)/2$. The number of vortices is then decreased by one at this field and the energy drops as shown by the arrows in Fig. 3. The magnetization calculated from Eq. (8) is shown by the lower curve in Fig. 5. It shows clearly a paramagnetic behavior, although it disagrees quantitatively with experiments and the numerical simulations based on the exact solution of the Ginzburg-Landau equations. This discrepancy results from the rather unrealistic London limit we used for systems for which $\kappa\sim0.3$ in order to obtain an analytic expression for the Gibbs energy. We emphasize that the system is not at thermal equilibrium but in a metastable state. It is worth noticing that for values of the parameter $\phi_1=\mathcal{E}'/2\pi=\ln R/\xi\sim2$, the paramagnetic Meissner effect can be observed as well for an equilibrium configuration, i.e., for a minimum of the Gibbs free energy. But this corresponds to $R\sim\xi$ so that the deltalike vortex approximation, crucial for the present discussion, is not justified.

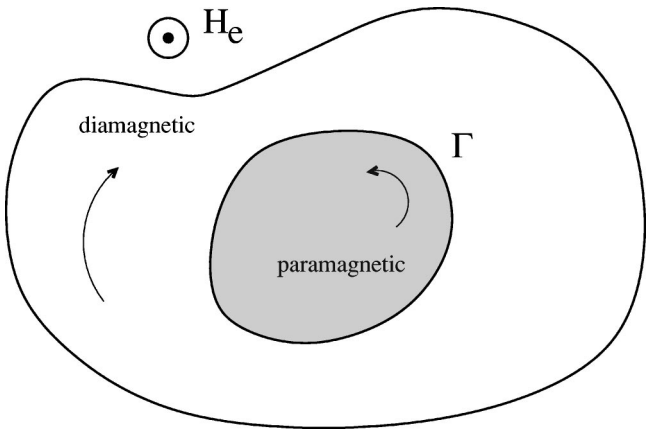

FIG. 6. Paramagnetic and diamagnetic zones separated by the curve Γ.

V. TOPOLOGICAL PHASE TRANSITIONS BETWEEN METASTABLE VORTEX PATTERNS

Up to now, we have considered vortex configurations for which the position x of the vortex ring was given by Eq. (31) resulting from the minimization of the energy. We shall now relax this condition and study the behavior of the metastable

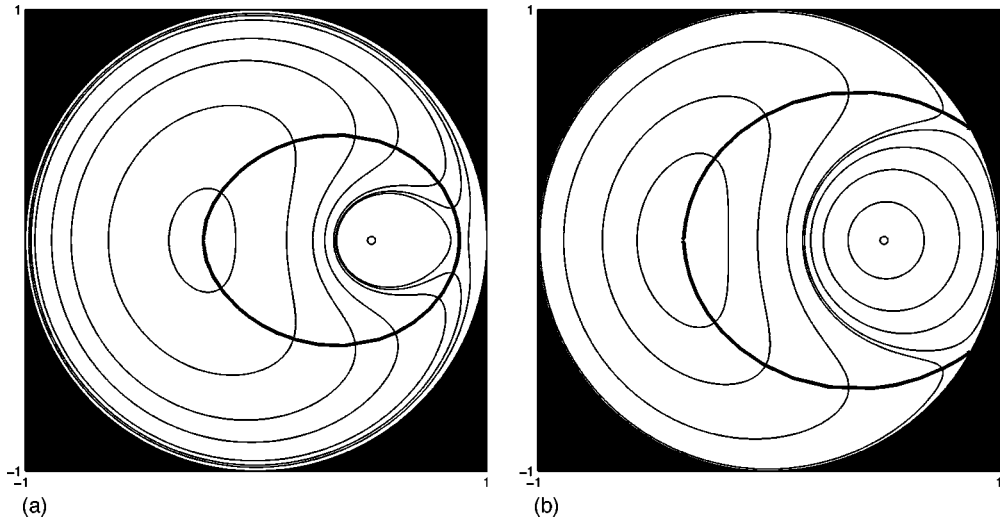

FIG. 7. The case of one single vortex ($N=1$). Behavior of the curve Γ for (a) $\phi_e>\phi_M(1)$ and (b) $\phi_m(1)<\phi_e<\phi_M(1)$.

vortex patterns as a function of the applied magnetic flux ϕ_e. Physically, this corresponds to a situation where N vortices are pinned by a potential and remain on fixed positions.

A. An effective Hamiltonian system

When varying the field ϕ_e, transitions in a vortex pattern with fixed number N of vortices will appear. To characterize them, we shall study the behavior of the magnetic field h given by Eq. (29). To that purpose, it is interesting first to notice that, in two dimensions, the Maxwell-Ampère equation $\vec{j}=\vec{\nabla}\times h\hat{z}$ is the Hamilton equation of a system whose generalized coordinates (p,q) are the coordinates (x,y) such that $j_x=\dot{x}, j_y=\dot{y}$ and the canonically conjugated momentum:

$$\dot{p}=-\partial_q h$$
$$\dot{q}=\partial_p h. \tag{40}$$

Then, the magnetic field corresponds to the Hamiltonian of the system and the current lines are the phase space trajectories. For a Hamiltonian system, the flow can be characterized by its critical (fixed) points at which

$$\vec{\nabla} h=0. \tag{41}$$

Using Eq. (40), we see that critical points correspond to zero velocity points such that $\vec{j}=0$.

In such a description, a vortex corresponds to a maximum in phase space. However, there also exist in the system other critical points, such as minima and saddle points. The number $N_M=N$ of maxima (i.e., vortices), N_m of minima, and N_s of saddles are not independent, because of the Euler-Poincare relation,[20] namely the Euler-Poincaré characteristic χ, is given by

$$\chi=N_M-N_s+N_m. \tag{42}$$

The integer χ is a topological invariant and is equal to 1 for a disk thus providing a constraint between the numbers of the different types of critical points. Hence, for a system with a given number of vortices, the difference N_s-N_m between saddles and minima is fixed. However, each of them can vary and the set of these numbers provides a complete description of the topology of the vortex configurations, namely each topological phase can be described using this set of integers.

A different way to encode the position and the distribution of the critical points of the magnetic field in the disk is to use a special contour Γ, introduced in Ref. 10 The curve Γ is defined by the condition that at each point $\vec{r}$ it is perpendicular to the current density $\vec{j}(\vec{r})$. The equation of Γ is then

$$\frac{dr}{d\theta}=r^2\frac{\partial_r h}{\partial_\theta h}. \tag{43}$$

To this definition we must add the requirement that Γ must pass through the critical points at which $\vec{j}(\vec{r})=0$. The curve Γ has several branches; one of them encircles all the vortices and defines a natural boundary between the diamagnetic (Meissner) domain near the boundary and the inner paramagnetic domain which includes the vortices (Fig. 6). An example of this curve is shown in Fig. 7 for the case of a single vortex.

The study of the critical points and the resulting behavior of Γ provides a complete description of the vortex states either for thermodynamic or metastable states and of the transitions between different sets of topological numbers when varying the applied field. From the behavior of the curve Γ as a function of the applied field ϕ_e, it might be interesting to draw the analogy with the pressure exerted on a closed membrane separating two systems.

B. Topological study of a polygonal distribution of vortices

We now consider the simple case where the cores of the vortices are placed on regular polygon at a distance x from the center of a cross section of the cylinder. The critical points can be classified (see Appendix C) according to their stability properties, obtained from the Hessian matrix $H_{ij}=\partial_i\partial_j h$. We review the various topological structures obtained and the transitions between them.

For a ring configuration of N vortices located at the distance x from the center the general expression (26) for the field h in circular coordinates r, θ reads

$$h=\phi_e(r^2-1)+\ln\left(\frac{1-2x^N r^N\cos N\theta+x^{2N}r^{2N}}{x^{2N}-2x^N r^N\cos N\theta+r^{2N}}\right). \tag{44}$$

At the critical point the partial derivatives of h vanish. The condition $\partial_r h=0$ leads to

$$\phi_e r-N(x^{2N}-1)r^{N-1}\,\frac{x^N\cos N\theta(r^{2N}+1)-(x^{2N}+1)r^N}{(1-2x^N r^N\cos N\theta+x^{2N}r^{2N})(x^{2N}-2x^N r^N\cos N\theta+r^{2N})}=0 \tag{45}$$

while the condition $\partial_\theta h=0$ rewrites as

$$Nr^N\sin N\theta\,\frac{(1-x^{2N})(1-r^{2N})}{(1-2x^N r^N\cos N\theta+x^{2N}r^{2N})(x^{2N}-2x^N r^N\cos N\theta+r^{2N})}=0. \tag{46}$$

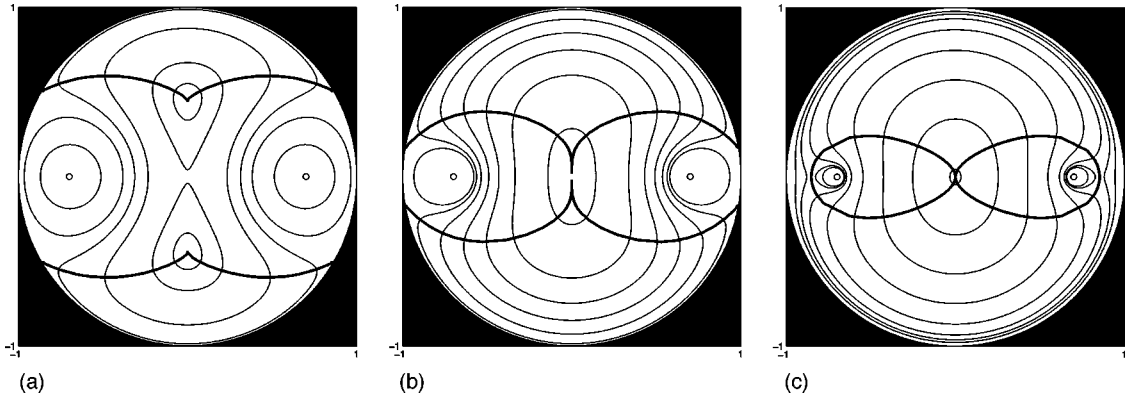

FIG. 8. The case of $N=2$ vortices for (a) $\phi_m(2)<\phi_e<\phi_c(2)$, (b) $\phi_c(2)<\phi_e<\phi_M(2)$, and (c) $\phi_e>\phi_M(2)$. The curve Γ is shown. The position of the vortices is taken to be $x=0.7>\sqrt{2-\sqrt{3}}$, therefore $\phi_c(2)<\phi_M(2)$.

The solutions of Eqs. (45) and (46) are studied in detail in Appendix C. One main feature is that one has to distinguish between the cases $N=1$, $N=2$, and $N>2$ where N is the number of vortices. We now describe these three cases separately.

1. Metastable configurations for N=1

For one single metastable vortex located at distance x from the center there is no other critical point for weak flux $\phi_e<\phi_m(1)$, with

$$\phi_m(1)=\frac{1-x}{1+x}. \tag{47}$$

At $\phi_e=\phi_m(1)$ a critical point appears at the point $r=1,\theta=-\pi$. For a flux slightly above $\phi_m(1)$, this point splits into a minimum at $r<1,\theta=-\pi$ and two saddle points on the boundary $r=1$ situated symmetrically about the diameter passing through the vortex. As the flux increases the minimum moves towards the center and the saddle points approach the point $r=1,\theta=0$ each from its side. They coalesce at this point for $\phi_e=\phi_M(1)$, where

$$\phi_M(1)=\frac{1+x}{1-x} \tag{48}$$

and for larger values of the flux one saddle point appears inside a section of the cylinder between the vortex and the boundary in the interval $x<r<1,\theta=0$. When $\phi_m(1)<\phi_e<\phi_M(1)$, the definition (42) must be generalized to the case of critical point on the boundary.[20] It becomes

$$\chi=N_M-N_s+N_m-\frac{1}{2}N_{sb}, \tag{49}$$

where N_{sb} is the number of saddle points on the boundary. Thus the index is again equal to 1.

An efficient way to visualize these transitions is to examine the changes in the curve Γ as the magnetic flux varies. In the case $\phi_e>\phi_M(1)$, shown in Fig. 7(a), the curve Γ lies inside the section of the cylinder and separates the paramagnetic (internal) and diamagnetic (external) regions. For $\phi_e=\phi_M(1)$ the saddle point reaches the boundary of the section and for $\phi_m(1)<\phi_e<\phi_M(1)$ the curve Γ starts and ends on the saddle points on the boundary [see Fig. 7(b)]. Therefore, in this regime, one cannot define a paramagnetic region inside the cylinder and there is no closed curve that encloses a unit of flux. There appears an arc of circle on the boundary where the direction of the current flow is opposite to the screening current responsible for the Meissner effect. At $\phi_e=\phi_m(1)$ the entire system becomes paramagnetic and the curve Γ disappears.

2. Metastable configurations for N=2

For low enough field $\phi_e<\phi_m(2)$, with

$$\phi_m(2)=2\frac{1-x^2}{1+x^2}, \tag{50}$$

the only critical point is a saddle point at the center. For $\phi_m(2)<\phi_e<\phi_M(2)$, where

$$\phi_M(2)=2\frac{1+x^2}{1-x^2}, \tag{51}$$

there are two minima situated symmetrically on the diameter perpendicular to the line passing through the vortices and two pairs of saddle points on the boundary. This configuration is shown in Fig. 8(a). Each pair is symmetric with respect to the line passing through the vortices and moves towards the points $r=1$, $\theta=0$, or $\theta=\pi$. For $\phi_e>\phi_M(2)$ each pair disappears and gives birth to one single saddle point located between a vortex and the boundary at $\theta=0$ or π as shown in Fig. 8(c).

Two minima inside the section move towards the center and at the critical value of the flux $\phi_e=\phi_c(2)$, where $\phi_c(2)=(1-x^4)/x^2$ they merge with the central point, which becomes a minimum for $\phi_e>\phi_c(2)$. This critical value can be shown to be always greater than $\phi_m(2)$, but it can be greater or less than $\phi_M(2)$ depending on the value of x. For $x<\sqrt{2-\sqrt{3}}\approx 0.52$, one has $\phi_c(2)>\phi_M(2)$, while for $x>\sqrt{2-\sqrt{3}}$, we have $\phi_c(2)<\phi_M(2)$. The latter case is shown in Figs. 8(b) and (c).

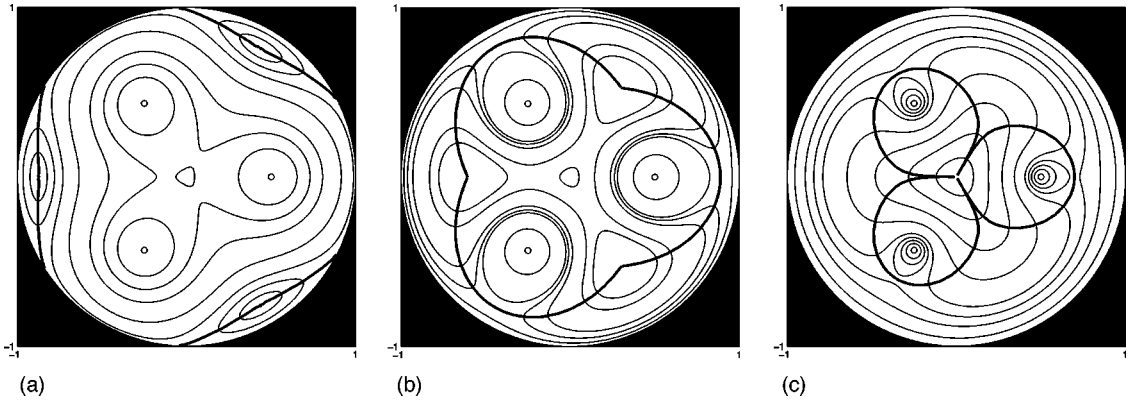

FIG. 9. The case of $N=3$ vortices for (a) $\phi_m(3)<\phi_e<\phi_M(3)$, (b) $\phi_M(3)<\phi_e<\phi_c(3)$, and (c) $\phi_e>\phi_c(3)$. The curve Γ is shown.

3. The case N>2: topological phase transitions

In that case, the central point is a minimum for all values of ϕ_e. In addition for low enough external flux there are N saddle points inside the section situated symmetrically at $\theta=2\pi(k+1/2)/N$. As the external flux is increased through $\phi_m(N)$, where

$$\phi_m(N)=N\frac{1-x^N}{1+x^N}. \tag{52}$$

N pairs of saddle points on the boundary appear together with N minima in the bulk [see Fig. 9(a)]. The minima move towards the center along the line defined by $\theta=2\pi(k+1/2)/N, k=1,\ldots,N$, while two saddle points constituting the kth pair move symmetrically to the points $\theta=2\pi k/N$ and $\theta=2\pi(k+1)/N$ as the flux increases in the interval $\phi_m(N)<\phi_e<\phi_M(N)$. When $\phi_e=\phi_M(N)$, with

$$\phi_M(N)=N\frac{1+x^N}{1-x^N}, \tag{53}$$

pairs of saddle points meet at $\theta=2\pi k/N$ and for larger values of the flux there are N saddle points situated between a vortex and the boundary. In this regime there are $N+1$ minima and $2N$ saddle points inside the section as shown in Fig. 9(b).

At $\phi_e=\phi_c(N)$, where $\phi_c(N)$ is given by the formulas (C9) and (C10), each of the N minima coalesce with each of the N saddle points at $r=\rho_c^{1/N}, \theta=2\pi(k+1/2)/N$, where ρ_c is given by Eq. (C9). For $\phi_e>\phi_c(N)$ there remains only one minimum in the center and N saddle points. It can be shown that $\phi_c(N)$ is always greater than $\phi_M(N)$ for $N>2$.

Then, for $\phi_e=\phi_c(N)$ a topological transition occurs, when a minimum and a saddle point coalesce. This transition and the corresponding curve Γ is depicted in Figs. 9(b) and (c). It is seen that the curve Γ undergoes itself a topological transition. For $\phi_e<\phi_c(N)$ it does not touch the center and has a topology of a ring, while for $\phi_e>\phi_c(N)$ it has a form of petals of a flower emanating from the center of the section.

C. A dynamical interpretation of the curve Γ

The curve Γ, defined above as being everywhere normal to the current flow, has a simple interpretation in terms of an effective dynamical system, which gives an alternative method to compute it. Instead of the Hamiltonian flow (40), consider the lines of $\vec{\nabla}h$, obtained from those of $\vec{j}$ by a rotation of 90°. This flow is clearly non-Hamiltonian and possess fixed points which are not present in the Hamiltonian dynamics, e.g., the positions of the vortices appear in this picture as a pointlike sources, though a saddle remain a saddle in this transformation. Then, the curve Γ represents a limit cycle of the flow $\vec{\nabla}h$ emanating from the saddle point. This is illustrated in Fig. 10 where it is clearly seen that the same curve as in Fig. 7(a) appears as a limit of the lines of $\vec{\nabla}h$.

VI. CONCLUSION

In this paper we have presented two different aspects of vortex patterns in a mesoscopic superconductor. First we focused on equilibrium properties of a type-II superconductor in the London regime. In this case, the Ginzburg-Landau equations reduce to a single linear elliptic equation that can

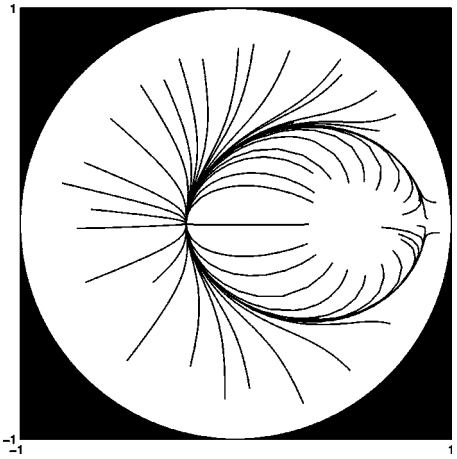

FIG. 10. The curve Γ as the limit cycle of the flow $\vec{\nabla}h$. The parameters are the same as in Fig. 7(a).

explicitly be solved in simple geometries. We have derived closed expressions for the free energy and the magnetization of a mesoscopic system which have been obtained as limiting cases of a general calculation valid for a system of any size[14] and not from specific assumptions related to the mesoscopic regime.[7] With these formulas, we have been able to study precisely the matching fields and to compute the paramagnetic Meissner effect, resulting from the existence of metastable states. The second part of the paper has been devoted to the general and topological study of the metastable states using a parallel with the theory of two-dimensional dynamical systems. We showed that a vortex pattern can be characterized by a set of topological integers, the number of vortices being one of them. Any change in this set corresponds to a topological transition of the vortex pattern. We calculated the critical fields associated with these transitions and we gave a dual interpretation of these transitions. A key concept is the introduction of a special curve Γ, that embodies the main geometric features of a configuration of vortices. This curve, which appears mathematically as a limit cycle of the system of currents generated by the vortex pattern, has a simple physical meaning: it separates paramagnetic from diamagnetic domains.

We emphasize that this approach that focuses on topological aspects are generic and can be extended, at least in a qualitative manner, to systems beyond the London regime and with different shapes. Here, we considered a circular cylinder to obtain simple analytical expressions. In recent studies, analytic expressions for the free energy of a cylinder with an elliptic cross section were found in the mesoscopic limit[24] and, more generally, an electrostatic analogy was developed that enables to study mesoscopic superconductors in the London regime with the help of conformal transformations;[25] using such tools, it would be interesting to carry on a quantitative study of topological phase transitions in arbitrary domains. A more challenging problem would be to study vortex patterns in a thin flat disc; indeed the shape and the interaction of vortices in the London limit are different from those studied here[19,21] and demagnetization effects will enhance the value of the field on the boundary of the sample. However, we believe that the topological results obtained here are robust, and will remain qualitatively unchanged as long as the topology of the sample itself is not modified.[22]

In this work, only static configurations of vortices have been investigated. A natural extension of the concepts introduced here would be to consider the dynamics of a vortex pattern, where a vortex would move in the field generated by the other vortices. In this context, the study of the deformations of the curve Γ would certainly shed some light on the mechanism of vortex nucleation in a superconducting system.

ACKNOWLEDGMENTS

E.A. and D.M.G. would like to thank Mark Mineev for fruitful and stimulating discussions. D.M.G. would like to thank SPhT at Saclay for hospitality. This research was supported in part by the U.S.-Israel Binational Science Foundation (BSF), by the Minerva Center for Non-linear Physics of Complex Systems, by the Israel Science Foundation, by the Niedersachsen Ministry of Science (Germany), and by the Fund for Promotion of Research at the Technion.

APPENDIX A: MAGNETIC INDUCTION IN A CYLINDER

We present the solution of the London Eq. (15) for the magnetic induction

$$\nabla^2 h(\vec{r}) - 2h(\vec{r}) = -4\pi \sum_{k=1}^{N} \delta(\vec{r} - \vec{r}_k) \tag{A1}$$

with the boundary condition $h(R,\theta) = h_e$. The polar coordinates are convenient for this geometry. Equation (A1) with a vanishing right-hand side describes the Meissner regime in the absence of vortices. The corresponding solution of the homogeneous equation is given by the θ-independent function

$$h_M(r) = h_e \frac{I_0(\sqrt{2}r)}{I_0(\sqrt{2}R)}, \tag{A2}$$

where the functions $I_n(x), K_n(x)$ are modified Bessel functions of first and second kind of order n which provide the regular and singular solutions respectively of Eq. (A1). The solution of the inhomogeneous Eq. (A1) for N vortices is written as a sum of the solution of the homogeneous equation and a particular solution:

$$h(r,\theta) = h_M(r) + h_V(r,\theta) + h_{\overline{V}}(r,\theta), \tag{A3}$$

where $h_V(r,\theta)$ is the solution for N vortices in the unbound domain

$$h_V(r,\theta) = 2\sum_{k=1}^{N} K_0(\sqrt{2}|\vec{r} - \vec{r}_k|) \tag{A4}$$

and the term $h_{\overline{V}}(r,\theta)$ is introduced to take care of the boundary conditions:

$$\begin{aligned} h_{\overline{V}}(R,\theta) &= -h_V(R,\theta) \\ &= -2\sum_{k=1}^{N} K_0(\sqrt{2[R^2 + r_k^2 - 2Rr_k\cos(\theta - \theta_k)]}). \end{aligned} \tag{A5}$$

On the other hand, the field $h_{\overline{V}}$ can be written as a superposition of solutions of Eq. (A1) regular in the interior of the boundary:

$$h_{\overline{V}}(R,\theta) = \sum_{n=-\infty}^{+\infty} c_n I_n(\sqrt{2}r) e^{in\theta}, \tag{A6}$$

where, since the field is real, the relation $c_{-n} = c_n^*$ holds. Expanding the left-hand side (lhs) of Eq. (A5) into Fourier series using standard identities of Bessel functions[23] we get

$$K_0(\sqrt{2[R^2+r_k^2-2Rr_k\cos(\theta-\theta_k)]}) = \sum_{n=-\infty}^{+\infty} K_n(\sqrt{2}R)I_n(\sqrt{2}r_k)e^{in(\theta-\theta_k)}. \quad \text{(A7)}$$

Equating the coefficients of the expansion of both sides of Eq. (A5) one obtains

$$c_n=\frac{K_n(\sqrt{2}R)I_n(\sqrt{2}r_k)}{I_n(\sqrt{2}R)}e^{-in\theta_k} \quad \text{(A8)}$$

from which the expression (20) follows immediately.

APPENDIX B: EXPRESSION OF THE GIBBS ENERGY FOR A CYLINDER

One takes advantage of the vector identity $(\nabla\times\vec{h})\cdot(\nabla\times\vec{h})=\nabla\cdot(\vec{h}\times\nabla\times\vec{h})+\vec{h}\cdot(\nabla\times\nabla\times\vec{h})$ to rewrite $(\nabla\times\vec{h})\cdot(\nabla\times\vec{h})=\nabla\cdot(\vec{h}\times\nabla\times\vec{h})-\vec{h}\nabla^2\vec{h}$, since $\nabla\cdot\vec{h}=0$. Then one uses the London equation (15) to rewrite the expression (12) for the free energy as

$$\mathcal{F}=\pi\sum_{k=1}^{N}\int_\Omega d^2r\, h(\vec{r})\,\delta(\vec{r}-\vec{r}_k)+\frac{1}{4}\int_\Omega d^2r\,\nabla\cdot(\vec{h}\times\nabla\times\vec{h}). \quad \text{(B1)}$$

The singular part $\mathcal{F}_\infty$ is obtained from the contribution of h_V to the first integral. The regular contribution to the free energy can be written using Stokes theorem:

$$\mathcal{F}-\mathcal{F}_\infty=\pi\sum_{k=1}^{N}h_M(\vec{r}_k)+\pi\sum_{k=1}^{N}h_{\overline{V}}(\vec{r}_k) +\frac{R}{4}\int_0^{2\pi}d\theta\,h(R,\theta)h_r(R,\theta), \quad \text{(B2)}$$

where h_r denotes the partial derivative of $h(r,\theta)$ with respect to r and the fields h_M and $h_{\overline{V}}$ are given by Eqs. (18) and (20). In the last term $h(R,\theta)=h_e$ can be taken out of the integration sign and the integral becomes

$$2\pi\frac{dh_M(R)}{dR}+2\pi\frac{\partial}{\partial R}\int_0^{2\pi}d\theta[h_V(R,\theta)+h_{\overline{V}}(R,\theta)] =2\sqrt{2}\pi h_e\frac{I_1(\sqrt{2}R)}{I_0(\sqrt{2}R)}-4\sqrt{2}\pi\sum_{k=1}^{N}\frac{I_0(\sqrt{2}r_k)}{I_0(\sqrt{2}R)} \times[I_0(\sqrt{2}R)K_1(\sqrt{2}R)+K_0(\sqrt{2}R)I_1(\sqrt{2}R)]. \quad \text{(B3)}$$

To prove the last equality the properties of the Bessel functions $I_0'(x)=I_1(x), K_0'(x)=-K_1(x)$, and the expansion (A7) were used. Only $n=0$ term contributes to the angular integral. Using another property of Bessel functions $I_0(x)K_1(x)+K_0(x)I_1(x)=1/x$ and one obtains that

$$\frac{h_eR}{4}\int_0^{2\pi}d\theta\,h_r(R,\theta)=\frac{\sqrt{2}\pi Rh_e^2}{2}\frac{I_1(\sqrt{2}R)}{I_0(\sqrt{2}R)} -\pi\sum_{k=1}^{N}h_e\frac{I_0(\sqrt{2}r_k)}{I_0(\sqrt{2}R)}. \quad \text{(B4)}$$

We notice that the contribution from the Meissner field h_M in Eq. (B1) exactly cancels with the second term in the last equation. Hence the regular part of free energy becomes

$$\mathcal{F}-\mathcal{F}_\infty=\sqrt{2}\pi Rh_e^2\frac{I_1(\sqrt{2}R)}{I_0(\sqrt{2}R)}-2\pi\sum_{n=-\infty}^{+\infty}\sum_{j,k=1}^{N} \times\frac{K_n(\sqrt{2}R)I_n(\sqrt{2}r_j)I_n(\sqrt{2}r_k)}{I_n(\sqrt{2}R)}\cos n(\theta_j-\theta_k). \quad \text{(B5)}$$

The term containing the average magnetic induction over the cross section of the cylinder is evaluated along the same lines, using the London Eq. (15):

$$h_e\int_\Omega h(\vec{r})d^2r=2\pi Nh_e+\frac{h_e}{2}\int_\Omega\nabla\cdot\nabla h(\vec{r})d^2r =\sqrt{2}\pi Rh_e^2\frac{I_1(\sqrt{2R})}{I_0(\sqrt{2})R} +2\pi h_e\sum_{k=1}^{N}\left(1-\frac{I_0(\sqrt{2r_k})}{I_0(\sqrt{2})}R\right). \quad \text{(B6)}$$

Using the expressions (B5) and (B6) in the definition (22) of the Gibbs energy completes the derivation of Eq. (24).

APPENDIX C: STUDY OF THE CRITICAL POINTS

In order to study critical points of the Hamiltonian system defined in Sec. V A, one has to solve Eqs. (45) and (46) for a given number N of vortices.

1. Existence and location of the critical points

We first look for critical points which are neither on the boundary of the section nor at the center, i.e., we concentrate on the generic position $0<r<1$. When $0<r<1$, one deduces that Eq. (46) is satisfied if $\sin N\theta=0$, i.e., when $\theta=k\pi/N$ for $k=0,1,\ldots,2N-1$. These values of the angle can be subdivided into two groups according to the sign of $\cos N\theta$. We now discuss the solution of Eq. (45) for the two cases separately.

a. Bulk critical points such that cos Nθ=+1

In this case, we are looking for ''parallel'' critical points that lie in the same direction as the vortices. And we shall prove that for any N, there exists a critical field $\phi_M(N)$, defined as follows:

$$\phi_M(N)=N(1+x^N)/(1-x^N), \quad \text{(C1)}$$

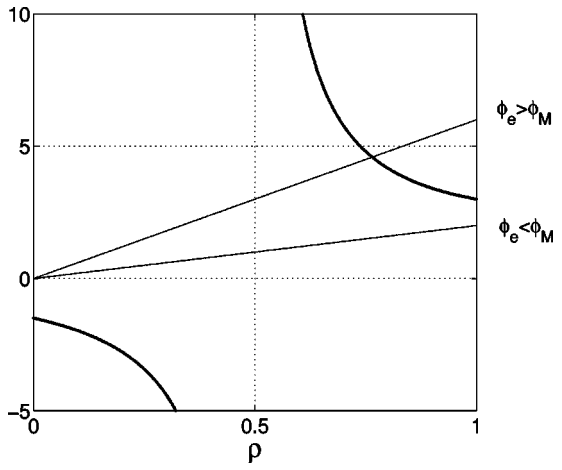

FIG. 11. Graphical solution of Eq. (C2) for one single vortex ($N=1$). The position of the vortex is taken to be $x=0.5$.

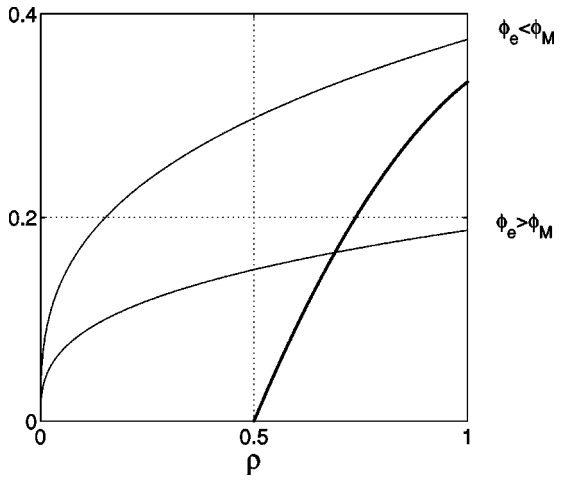

FIG. 12. Graphical solution of the equation (C3) for $N>2$ vortices. The position of the ring of vortices is taken to be $x=0.5$.

such that when $\phi_e>\phi_M(N)$ there is always a critical point between each vortex and the boundary, and no such point exists if $\phi_e<\phi_M(N)$.

Using the new variables $\xi=x^N$ and $\rho=r^N$ Eq. (45) reduces to

$$\frac{\phi_e}{N}\rho^{(2/N)-1}=\frac{\xi^2-1}{(1-\xi\rho)(\xi-\rho)}. \tag{C2}$$

Looking at this equation, it is clear that systems with $N=1$, $N=2$, or $N>2$ should be discussed separately.

For $N=1$, the plots of the left- and right-hand sides of this equation are represented in Fig. 11. They cross for $\rho<1$ only if the rhs evaluated at $r=1$ is less than ϕ_e, i.e., for $\phi_e>\phi_M=(1+\xi)/(1-\xi)=(1+x)/(1-x)$. In this case the solution of Eq. (C2) can be shown to exist using the continuity of the functions. The position of the critical point corresponding to this solution satisfies $\xi<r<1$, i.e., the point resides between the vortex and the boundary. For $\phi_e<\phi_M$ there is no solution.

For $N\geqslant 2$, it is worthwhile to consider the reciprocal of Eq. (C2) which rewrites as

$$\frac{N}{\phi_e}\rho^{1-(2/N)}=\frac{1}{\xi^2-1}(1-\xi\rho)(\xi-\rho). \tag{C3}$$

The right-hand side is a convex parabola with zeros at $\xi<1$ and $1/\xi>1$. For $N=2$ the lhs is a constant function and it is clear that if $\phi_e>\phi_M=2(1+\xi)/(1-\xi)=2(1+x^2)/(1-x^2)$ there is always a solution for $\xi<\rho<1$, therefore there exists a critical point between the vortex and the boundary, while $\phi_e<\phi_M$ no solution exists. For $N>2$ the lhs is an increasing fractional power of ρ (see Fig. 12). Equation (C3) always has a solution between ξ and 1 if $\phi_e>\phi_M=N(1+\xi)/(1-\xi)=N(1+x^N)/(1-x^N)$ and no solution if $\phi_e<\phi_M$.

b. Bulk critical points such that $\cos N\theta=-1$

We are now looking for ''antiparallel'' critical points that lie in a direction bisecting the angle between two neighboring vortices. Here the discussion is more involved:

When $N=1$ there appears a critical field $\phi_m(1)=(1-x)/(1+x)$ such that when $\phi_e>\phi_m(1)$ there exists a critical point in the direction opposite to the vortex whereas when $\phi_e<\phi_m(1)$ no such point exists.

When $N=2$, there are two critical fields $\phi_m(2)$ and $\phi_c(2)$ such that when $\phi_m(2)<\phi_e<\phi_c(2)$ there are exactly two antiparallel critical points and there are no such points when $\phi_e<\phi_m(2)$ or $\phi_e>\phi_c(2)$.

When $N>2$, one has again two critical fields $\phi_m(N)$ and $\phi_c(N)$ such that when $\phi_e<\phi_m(N)$ there exist N antiparallel critical points, when $\phi_m(N)<\phi_e<\phi_c(N)$, there are $2N$ such points, and when $\phi_e>\phi_c(N)$, there are no antiparallel critical points.

We now prove these assertions and calculate the corresponding critical fields.

Consider first that $N=1$; then Eq. (45) in terms of the variables ρ and ξ becomes

$$\phi_e\rho=\frac{1-\xi^2}{(1+\xi\rho)(\xi+\rho)} \tag{C4}$$

and a solution exists in the interval $0<\rho<1$ if the value of the lhs at $\rho=1$ exceeds the value of the rhs at the same point, as shown in Fig. 13. This happens for $\phi_e>\phi_m(1)=(1-x)/(1+x)$.

Now, when $N\geqslant 2$, the Eq. (45) can be rewritten as

$$\frac{N}{\phi_e}\rho^{1-2/N}=\frac{1}{1-\xi^2}(1+\xi\rho)(\xi+\rho). \tag{C5}$$

$N=2$: this case is illustrated in Fig. 14. For $\phi_e<\phi_m(2)=2(1-\xi)/(1+\xi)=2(1-x^2)/(1+x^2)$ there is no solution, for $\phi_e=\phi_m(2)$ one solution appears at $\rho=1$ and it persists for

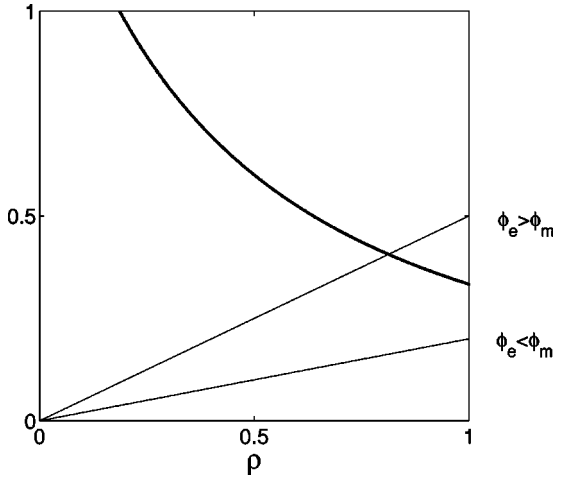

FIG. 13. Graphical solution of Eq. (C4) for one single vortex ($N=1$). The position of the vortex is taken to be $x=0.5$.

the range of the flux $\phi_m(2)<\phi_e<\phi_c(2)=2(1-\xi^2)/\xi=2(1-x^4)/x^4$. For higher flux, $\phi_e>\phi_c(2)$, this solution disappears at $\rho=0$.

The case $N>2$ is the most interesting: Fig. 15 shows the behavior of both sides of Eq. (C5). Comparing the value of the lhs at $\rho=1$ with that of the rhs and using the fact that $\rho^{1-2/N}$ has a negative curvature, while that of the rhs is always positive, we can state that for $\phi_e<\phi_m(N)$, where

$$\phi_m(N)=N(1-\xi)/(1+\xi)=N(1-x^N)/(1+x^N) \quad \text{(C6)}$$

there is only one solution. Another solution appears at $\rho=1$ for $\phi_e=\phi_m(N)$ and these two solutions move towards each other when the flux is increased in the interval $\phi_m(N)<\phi_e<\phi_c(N)$, whereas at the critical value of the flux $\phi_e=\phi_c(N)$ these two solutions coalesce. For $\phi_e>\phi_c(N)$, Eq. (C5) has no solutions in the interval $0<\rho<1$.

Calculation of the critical flux ϕ_c. For $\phi_e(N)=\phi_c$ the function $f_{\rm lhs}(\rho)=(N/\phi_e)\rho^{1-2/N}$ and $f_{\rm rhs}(\rho)=(1+\xi\rho)(\xi+\rho)/(1-\xi^2)$ are tangent at some point $\rho=\rho_c$ as shown in Fig. 15. Equating the value of these functions and the value of their derivatives at $\rho=\rho_c$ we obtain the following equations:

$$\phi_c(\rho_c+\xi)(1+\xi\rho_c)=N(1-\xi^2)\rho_c^{1-2/N}$$
$$\phi_c(2\xi\rho_c+\xi^2+1)=(N-2)(1-\xi^2)\rho_c^{-2/N}. \quad \text{(C7)}$$

Dividing the first equation by the second leads to the quadratic equation for ρ_c:

$$(N+2)\xi\rho_c^2+2(\xi^2+1)\rho_c-(N-2)\xi=0 \quad \text{(C8)}$$

which has the unique positive solution

$$\rho_c=\frac{-(1+\xi^2)+\sqrt{(1-\xi^2)^2+N^2\xi^2}}{(N+2)\xi}. \quad \text{(C9)}$$

The critical flux is obtained by substituting the value of ρ_c into the first equation of Eq. (C7):

$$\phi_c=\frac{N(1-\xi^2)\rho_c^{1-2/N}}{(\rho_c+\xi)(1+\xi\rho_c)}. \quad \text{(C10)}$$

We notice that for $N=2$ the formula (C9) yields the correct value $\rho_c=0$. Although topologically the cases $N=2$ and $N>2$ are different, the critical flux $\phi_c(2)=(1-\xi^2)/\xi$, as we shall see later, comes out correctly.

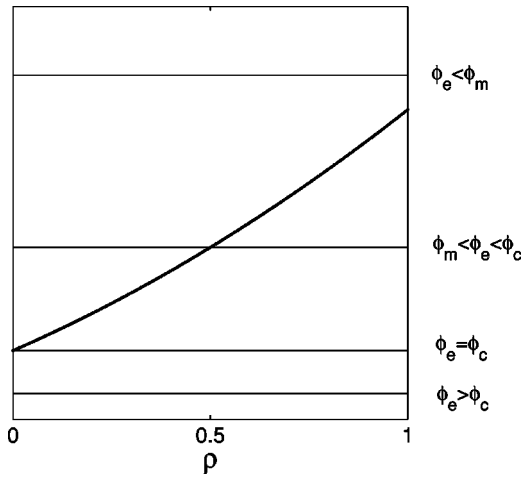

FIG. 14. Graphical solution Eq. (C5) for $N=2$ vortices. The position of each vortex is taken to be $x=0.5$.

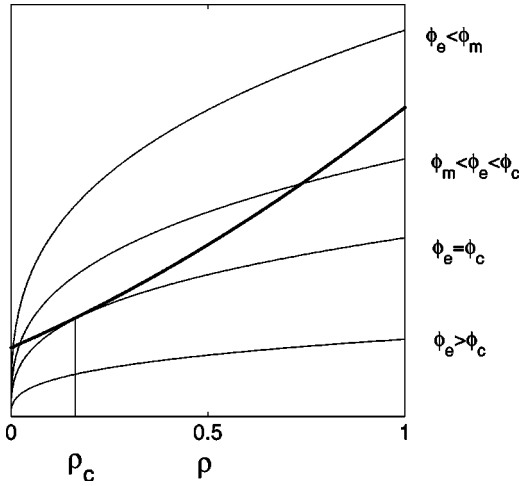

FIG. 15. Graphical solution of Eq. (C5) for $N>2$ vortices. The position of each vortex is taken to be $x=0.5$.

c. Central and boundary critical points

So far we did not discuss the two cases, $r=0$ and $r=1$. For $N=1$ the center, $r=0$, does not satisfy Eqs. (45) and (46) and therefore is not a critical point. For $N>1$ the value $r=0$ is always a solution of Eqs. (45) and (46). For the points on the boundary, $r=1$, Eq. (46) is always satisfied and substituting the value $r=1$ into Eq. (45) we find that there are $2N$ critical points on the boundary with an angle given by the following relation:

$$\cos N\theta=\frac{1}{2x^N}\left[1+x^{2N}-\frac{N(1-x^{2N})}{\phi_e}\right] \quad \text{(C11)}$$

which is meaningful only for values of the flux between $\phi_m(N)$ and $\phi_M(N)$.

2. The nature of the critical points

We now discuss the topological nature of the critical points and classify them by linearizing the stability exponents near each of these points. The problem is then reduced to the study of the Hessian matrix of the second derivatives

$$H=\begin{pmatrix} \partial_r^2 h & \partial_r\partial_\theta h \\ \partial_\theta\partial_r h & \partial_\theta^2 h \end{pmatrix}. \tag{C12}$$

Since at the critical points inside the section we have $\sin N\theta=0$ the mixed derivative vanish and the Hessian matrix is diagonal in polar coordinates. The second derivative with respect to θ is given at the critical points by

$$\partial_\theta^2 h=-2N^2\rho\frac{(1-\rho^2)(1-\xi^2)}{(1-\xi\rho)^2(\xi-\rho)^2}<0 \tag{C13}$$

for $\cos N\theta=+1$ and by

$$\partial_\theta^2 h=+2N^2\rho\frac{(1-\rho^2)(1-\xi^2)}{(1+\xi\rho)^2(\xi+\rho)^2}>0 \tag{C14}$$

for $\cos N\theta=-1$. The value of the second derivative with respect to r can be obtained by looking at the way the first derivative $\partial_r h$ changes sign near each solution of Eq. (45). We shall now discuss separately the nature of the critical points in the ''parallel,'' ''antiparallel,'' ''central,'' and ''boundary'' cases.

a. Bulk critical points with $\cos N\theta=+1$

For $\phi_e>\phi_M$, there is only one critical point at ρ_1 in the interval $\xi<r<1$. The results for the second derivatives at this point are summarized in the following table:

	$0<\rho<\rho_1$	$\rho_1<\rho<1$
$\partial_r h$	−	+
$\partial_r^2 h$	+	
$\partial_\theta^2 h$	−	
Crit. point	Saddle	

b. Bulk critical points with $\cos N\theta=-1$

The following tables provide a classification of critical points in a variety of regimes.

$N=1$. $\phi_e<\phi_m$: No critical points. $\phi_e>\phi_m$: One critical point at ρ_1.

	$0<\rho<\rho_1$	$\rho_1<\rho<1$
$\partial_r h$	−	+
$\partial_r^2 h$	+	
$\partial_\theta^2 h$	+	
Crit. point	Minimum	

$N=2$. $\phi_e<\phi_m$: No critical points. $\phi_m<\phi_e<\phi_c$: One critical point at ρ_1.

	$0<\rho<\rho_1$	$\rho_1<\rho<1$
$\partial_r h$	−	+
$\partial_r^2 h$	+	
$\partial_\theta^2 h$	+	
Crit. point	Minimum	

$\phi_e>\phi_c$. No critical points.

$N>2$. $\phi_e<\phi_m$: One critical point at ρ_1.

	$0<\rho<\rho_1$	$\rho_1<\rho<1$
$\partial_r h$	+	−
$\partial_r^2 h$	−	
$\partial_\theta^2 h$	+	
Crit. point	Saddle	

$\phi_m<\phi_e<\phi_c$: Two critical points at $\rho_1<\rho_2$.

	$0<\rho<\rho_1$	$\rho_1<\rho<\rho_2$	$\rho_2<\rho<1$
$\partial_r h$	+	−	+
$\partial_r^2 h$	−		+
$\partial_\theta^2 h$	+		+
Crit. point	Saddle		Minimum

$\phi_e>\phi_c$: No critical points.

c. Central and boundary critical points

Consider now the point $r=0$. Expanding the field $h(r,\theta)$ given by Eq. (44) for small r we obtain

$$h(r,\theta)\approx-(\phi_e-2N\ln x)+\phi_e r^2+2\cos(N\theta)\left(\frac{1-\xi^2}{\xi}\right)r^N. \tag{C15}$$

As we mentioned before, for $N=1$ the point $r=0$ is not a critical point (due to the presence of a term linear in r). For $N=2$, two last terms are quadratic in r and the character of the critical point depends on the value of the flux ϕ_e. For $\phi_e<\phi_c=(1-\xi^2)/\xi$ the center, $r=0$, is a saddle, while for $\phi_e>\phi_c$ it turns out to be to a minimum. This is to be compared with the prediction of formula (C10). It is interesting to notice that this happens when the minimum located along the line $\cos 2\theta=-1$ disappears at the center. For $N>2$, the last term in Eq. (C15) is negligible and the center is always a minimum.

When $\phi_m<\phi_e<\phi_M$ we must consider the critical points on the boundary. Since for $r=1$ the condition $\partial_\theta h=0$ is satisfied for all θ, we obtain $\partial_\theta^2 h=0$ and $\partial_r\partial_\theta h\neq 0$ if $\cos^2 N\theta\neq 1$, which is always satisfied for ϕ_e in the interval between ϕ_m and ϕ_M. Thus the determinant of the Hessian matrix (C12), given by $\det H=-(\partial_r\partial_\theta h)^2$, is negative and the eigenvalues are of opposite sign. We conclude that the critical points at the boundary are saddles.

[1] A.K. Geim, I.V. Grigorieva, S.V. Dubonos, J.G.S. Lok, J.C. Maan, A.E. Filippov, and F.M. Peeters, Nature (London) **390**, 259 (1997).

[2] C. Bolech, G.C. Buscaglia, and A. Lopez, Phys. Rev. B **52**, R15 719 (1995)

[3] P. Singha Deo, V.A. Schweigert, F.M. Peeters, and A.K. Geim, Phys. Rev. Lett. **79**, 4653 (1997).

[4] V.A. Schweigert, F.M. Peeters, and P. Singha Deo, Phys. Rev. Lett. **81**, 2783 (1998).

[5] J.J. Palacios, Phys. Rev. B **58**, R5948 (1998).

[6] R. Benoist and W. Zwerger, Z. Phys. B: Condens. Matter **103**, 377 (1997).

[7] A.I. Buzdin and J.P. Brison, Phys. Lett. A **196**, 267 (1994).

[8] P.A. Venegas and E. Sardella, Phys. Rev. B **58**, 5789 (1998).

[9] E.B. Bogomol'nyi, Yad. Fiz. **24**, 861 (1976) [Sov. J. Nucl. Phys. **24**, 449 (1976)]; D. Saint-James, E.J. Thomas, and G. Sarma, *Type II Superconductivity* (Pergamon Press, Oxford, 1969).

[10] E. Akkermans and K. Mallick, J. Phys. A **32**, 7133 (1999); E. Akkermans, D.M. Gangardt, and K. Mallick, Phys. Rev B. **62**, 12 427 (2000).

[11] A.K. Geim, S.V. Dubonos, J.G.S. Lok, M. Henini, and J.C. Maan, Nature (London) **396**, 144 (1998).

[12] C. Heinzel, T. Theilig, and P. Ziemann, Phys. Rev. B **48**, 3445 (1993).

[13] V.A. Schweigert and F.M. Peeters, Physica C **180**, 426 (2000).

[14] G. Böbel, Nuovo Cimento, **38**, 1740 (1965).

[15] V.A. Schweigert and F.M. Peeters, Physica C **144**, 266 (2000); A.K. Geim, S.V. Dubonos, J.J. Palacios, I.V. Grigorieva, M. Henini, and J.J. Schermer, Phys. Rev. Lett. **85**, 1528 (2000).

[16] P.G. de Gennes, *Superconductivity of Metals and Alloys* (Addison-Wesley, New York, 1989).

[17] A.A. Abrikosov, *Fundamentals of the Theory of Metals* (North-Holland, Amsterdam,1988).

[18] C.P. Bean and J.D. Livingston, Phys. Rev. Lett. **12**, 14 (1964).

[19] J. Pearl, Appl. Phys. Lett. **5**, 65 (1964).

[20] M. Morse, *Topological Methods in the Theory of Functions of a Complex Variable* (Princeton University Press, Princeton, NJ, 1947).

[21] A.L. Fetter, Phys. Rev. B **22**, 1200 (1980).

[22] For a discussion of topological aspects, see E. Akkermans and K. Mallick, in *Topological Aspects of Low Dimensional Systems*, Les Houches Lecture Notes, July 1998, Interéditions (Springer-Verlag, Berlin, 2000).

[23] M. Abramowitz and I.A. Stegun, *Handbook of Mathematical Functions* (Dover, New York, 1965).

[24] C. Meyers and M. Daumens (unpublished).

[25] A. Buzdin and M. Daumens, Physica C **332**, 108 (2000).